Groundwater

Distributed Temperature Sensing to Measure Infiltration Rates Across a Groundwater Recharge Basin

by Ricardo Medina[1], Christine Pham[2], Megan H. Plumlee[3], Adam Hutchinson[4], Matthew W. Becker[5], and Patrick J.O'Connell[6]

Abstract

Managed aquifer recharge is used to augment groundwater resources and provide resiliency to water supplies threatened by prolonged droughts. It is important that recharge facilities operate at their maximum efficiency to increase the volume of water stored for future use. In this study, we evaluate the use of distributed temperature sensing (DTS) technology as a tool to measure high-resolution infiltration rates at a large-scale recharge facility. Fiber optic cable was laid out inside a spreading basin in a spiral pattern, at two different depths. The cables measured the propagation of diurnal surface water temperature oscillations into the basin depth. The rate of heat propagation is proportional to the velocity of the water, making it possible to estimate the infiltration rate from the temperature measurements. Our results showed that the infiltration rate calculated from DTS, averaged over the entire basin, was within 5% of the infiltration rate calculated using a conventional metering method. The high-resolution data obtained from DTS, both spatially and temporally, revealed heterogeneous infiltration rates throughout the basin; furthermore, tracking the evolution of infiltration rates over time revealed regions with consistently high infiltration rates, regions with consistently low infiltration rates, and regions that evolved from high to low rates, which suggested clogging within that region. Water utilities can take advantage of the high-resolution information obtained from DTS to better manage recharge basins and make decisions about cleaning schedule, frequency, and extent, leading to improved basin management strategies, reduced O&M costs, and increased groundwater recharge.

Introduction

Managed aquifer recharge (MAR) is the practice of increasing, by artificial means, the amount of water entering a groundwater reservoir for later recovery as a drinking water supply or for environmental benefit. MAR can be used to store stormwater runoff, surface water runoff, and/or treated wastewater in aquifers for future use (Bouwer 2002; Dillon 2005, 2009; Fox 2007). One benefit of MAR is the large volume of groundwater that can be stored; for example, the Orange County Groundwater Basin (aquifer) can store up to 81.4×10^9 m^3 (66 million acre-feet) (Woodside and Westropp 2015). For comparison, Lake Elsinore, southern California's largest natural lake, can store 51.4×10^6 m^3 (41,700 acre-feet) and Lake Shasta, California's largest reservoir, can store 5.6×10^9 m^3 (4.5 million acre-feet). Furthermore, storing water in groundwater aquifers reduces evaporation losses (Kazner et al. 2012), prevents saltwater intrusion in coastal regions (Sherif and Hamza 2001; Khadra et al. 2017), and improves water quality through soil aquifer treatment (Drewes 2009; Dillon et al. 2010; Fox and Makam 2011).

There are several MAR methods, however, the appropriate method at any site depends on the local hydrogeology, water-source availability and reliability, water demand, and future use of the recovered water (Bouwer 2002; Dillon et al. 2010). The most common MAR methods include: aquifer storage and recovery (ASR), aquifer storage transfer and recovery (ASTR), infiltration galleries, riverbank filtration, and spreading

[1]Corresponding author: Research & Development, Orange County Water District, 4060 E. La Palma Ave., Anaheim, CA 92807; (714) 378-3303; rmedina@ocwd.com

[2]Research & Development, Orange County Water District, Anaheim, CA; cpham@ocwd.com

[3]Research & Development, Orange County Water District, Fountain Valley, CA; mplumlee@ocwd.com

[4]Orange County Water District, Fountain Valley, CA;, ahutchinson@ocwd.com

[5]Department of Geological Sciences, California State University, Long Beach, Long Beach, CA;, matt.becker@csulb.edu

[6]Department of Geological Sciences, California State University, Long Beach, Long Beach, CA;, pjoconnell4@gmail.com

Article impact statement: DTS technology can improve the management of spreading basins by providing spatial distribution of infiltration rates over time.

Received September 2019, accepted April 2020.

doi: 10.1111/gwat.13007

basins (also known as infiltration basins). Both ASR and ASTR use wells to inject water directly into the aquifer; ASR uses the same well for injection and extraction, while ASTR uses one well for injection and a second well, located at a distance, for extraction (Dillon 2009; Dillon et al. 2010). Drawbacks of these methods include the limited injection capacity, high operational cost, and the well's screen susceptibility to clogging which significantly reduces the effectiveness of ASR/ASTR (Martin 2013). Infiltration galleries are buried structures, for example, perforated conduits surrounded by highly permeable material, such as gravel, to facilitate water transport through the soil. Infiltration galleries are typically used in riverbank filtration to recharge river water or used in residential areas to capture rainfall runoff (Page et al. 2018). Riverbank filtration takes advantage of the natural landscape to recharge the aquifer, however, recharge is limited to the vicinity of the river and its natural flow. Spreading basins are man-made ponds that spread the water over relatively large areas and retain the water for some time before the water infiltrates (percolates) into the aquifer (Bouwer 1988, 2002). Disadvantages of spreading basins include (1) the potential for clogging, which requires routine maintenance and (2) the large footprint, which increases capital costs, especially in urban areas where land is expensive (Rice 1974; Bouwer and Rice 1989; Abel et al. 2015). Spreading basins are preferred due to their relatively low cost, the potential to store large volumes of water, easy operation, and the potential esthetic value added to the surrounding landscape. Furthermore, unlike other MAR techniques, spreading basins offer great versatility, for example, in addition to recharge, the basin can be used for flood protection and flood control or as a recreational area (Lopez et al. 2015; Bradshaw et al. 2019).

Incorporating spreading basins as part of a MAR operation requires continuous monitoring and maintenance to operate the basin at its optimal recharge rate. The infiltration rate of the basin and remaining storage capacity are key parameters for basin management. One method to measure the average infiltration rate of spreading basins is the mass balance or water balance (WB) method, which requires monitoring total inflow rate, water surface elevation or stage, storage volume, and wetted area. It is well known that the average infiltration rate of basins decline over time, due to clogging. Clogging is caused by physical, chemical, and biological processes that reduce the pore space available for water to move through, which leads to the formation of a low-permeability clogging layer at the bottom of the basin that significantly curtails the infiltration rate (Bouwer and Rice 1989). If a basin is actively managed, operators monitor the infiltration rate to determine when a basin has clogged, for example, when the average infiltration rate decreases to some predetermined value. Because the WB method provides an average infiltration rate for the entire basin, it is typically assumed the entire basin is clogged and remedial action is taken to restore infiltration rates to optimum levels (Becker et al. 2013). A common remediation strategy is to physically remove the clogging material by cleaning the bottom of the basin via scraping using heavy equipment. Recent studies have observed heterogeneous infiltration rates varying over space and time, challenging the assumption that recharge basins clog uniformly (Pidlisecky and Knight 2011; Racz et al. 2012; Becker et al. 2013). Thus, high-resolution infiltration rates (both spatial and temporal) may be important to manage the basin by providing information about localized areas impacted by clogging.

A recently introduced method to estimate infiltration rate uses temperature as a tracer to measure the velocity of water moving through the subsurface. This method tracks a heat front propagating through the subsurface underneath the basin floor. Heat propagation through saturated soils is assumed to be one-dimensional, driven by convection. This transport mechanism is described by analytical methods and used to obtain an accurate estimate of the moving front's velocity (Suzuki 1960; Stallman 1965). Using this method, researchers estimated the magnitude and direction of water moving in the hyporheic zone by using single point probes to measure the temperature at the streambed and at some depth below the surface. These fluxes were used to identify gaining and losing reaches of the stream and to understand processes in the hyporheic zone (Taniguchi 1993; Silliman et al. 1995; Becker et al. 2004; Conant 2004; Hatch et al. 2006; Constantz 2008; Koch et al. 2015). Single point temperature sensors provide a good estimate of fluxes in rivers and streams with little or no spatial variation in the crossflow direction, for example, where a single flux measurement is representative of the entire river width. However, in places where spatial variability may be expected, such as spreading basins, single-point sensors do not provide enough coverage to obtain high resolution fluxes. Furthermore, the use of single-point sensors is impractical and expensive. Therefore, it has been recently proposed to use fiber optic cables rather than single-point sensors to achieve such high-spatial resolution measurements.

Fiber optic distributed temperature sensing (DTS) has been used to quantify groundwater-surface water exchanges along large stream reaches (Selker et al. 2006; Lowry et al. 2007; Vogt et al. 2010; Briggs et al. 2012; Mwakanyamale et al. 2012; Hare et al. 2015). DTS sensors use backscatter to measure temperature, and time-of-flight to determine the location of the measurement (Tyler et al. 2009). Using diurnal temperature variation, Becker et al. (2013) observed DTS-measured infiltration rates compared favorably to WB estimates in a small (2 hectares) spreading basin. Taking advantage of the spatial resolution provided by DTS, Mawer et al. (2016) showed that approximately 80% of the recharged water infiltrated through 50% of a spreading basin site in Colorado. Beyond its applications for research or in limited, one-time site investigations, DTS technology has potential for integration as a tool to manage recharge facilities and optimize recharge operations as part of a data-driven MAR strategy, due to the high-resolution

infiltration rates both spatially and temporally. Better information regarding distributed infiltration rates may lead to better basin management strategies, augment the amount of groundwater recharge, and reduce operation and maintenance costs.

In this study, we present the results of a large-scale demonstration project using DTS to measure infiltration rates at a groundwater recharge facility. The objectives of the study were to: (1) evaluate fiber optic DTS technology as a tool to provide real-time monitoring of recharge rates at a groundwater recharge basin and (2) demonstrate the value of this technology to water utility managers by identifying areas of high and low percolation due to localized clogging. Though DTS has been previously used to measure infiltration rates at recharge facilities, to the authors' knowledge, this is the first time DTS data was collected for an extended period (over 2 years and ongoing) at a groundwater recharge facility. Furthermore, the present study is the first to use DTS to measure the infiltration rates of a newly constructed MAR facility since commissioning after it began consistently receiving treated water.

Materials and Methods

In this section we briefly describe the field site, the field installation of the DTS system, and the methods used to calculate infiltration rates.

Field Site Description

The Orange County Groundwater Basin (basin) underlies northern Orange County in southern California and covers approximately 900 km^2 (350 sq. miles). The aquifer is comprised of a complex series of interconnected sand and gravel deposit layers separated by low-permeability clay and silt deposits, or aquitards, forming a multilayer aquifer system (Figure 1b). These layers have been deposited over millennia by a combination of alluvial and marine deposition processes. In the coastal and central portions of the basin, the aquifer layers are hydraulically disconnected. These deposits are predominantly marine deposits, with alluvial deposits cutting through. In the inland areas (also known as the forebay area—from points B-C in Figure 1b), the clay and silt deposits become thinner and more discontinuous, allowing groundwater to flow between shallow and deeper aquifers (Hutchinson et al. 2013). These layers are predominantly alluvial, especially the upper layers (several hundred feet or more). Fluvial deposits in this area are highly permeable, with hydraulic conductivity as high as 91.4 meters/day or m/d (300 feet/d), making this region ideal for groundwater recharge.

Groundwater is the principal drinking water supply for north and central Orange County. The Orange County Water District (OCWD) is a groundwater management agency that replenishes the basin in the forebay area using 25 recharge facilities, 36 injection wells, and approximately 9.7 km (6 miles) of the Santa Ana River, near Anaheim, California. OCWD's recharge facilities cover 445 wet ha (1100 acres) and can store up to 32.3×10^6 m^3 (26,200 acre-feet) of water (Hutchinson et al. 2017). Figure 1a shows the location of the recharge facilities. The source of water used for recharge by OCWD includes Santa Ana River, imported water from the California State Water Project and Colorado River Aqueduct, and captured rainfall runoff. Another significant source of water for recharge is treated recycled water from OCWD's Groundwater Replenishment System Advanced Water Purification Facility (GWRS-AWPF). The AWPF treats secondary effluent from the Orange County Sanitation District using microfiltration, reverse-osmosis, and ultraviolet advanced oxidation process, and has a production capacity of 4.4 m^3/s (100 MGD). About ~1.3 m^3/s (30 MGD) of the advanced purified water is injected at the Talbert sea water intrusion barrier. Approximately 8.8×10^{-2} m^3/s (2 MGD) are injected in a well 4.5 km (2.8 miles) inland; the remaining ~3.1 m^3/s (70 MGD) is pumped 22.5 km (14 miles) inland to two spreading basins receiving exclusively GWRS water (Figure 1a). The practice of recharging recycled water into a groundwater aquifer is known as groundwater augmentation for (indirect) potable reuse.

Our study site, La Palma Basin, is a currently operated recharge basin. It is one of two basins operated by OCWD dedicated to the recharge of GWRS water, that is, no other sources, such as Santa Ana River water, are recharged in this basin. La Palma Basin is divided by a 1.5 m (5 ft) berm into two sub-basins, referred to as the North and South sub-basins. The basin has an approximate total wet area of 4.5 ha (11.0 acres) and an average depth of 3.0 m (10 ft). The basin floor grades 0.3% from southwest to northeast (Figure 1b). The native material of this site is mainly poorly graded alluvial sand from the Santa Ana River, with few interbedded layers of silt and clay (Moore 2014).

Field Installation of DTS Cables

Two co-located, fiber-optic cables, vertically separated by ~50.8 cm (20 inch) were installed in each subbasin, that is, one cable at depth and one at the basin floor (at the water-soil interface). The subsurface cable was installed using a ripper tool, mounted onto a tractor, which sliced into the basin sediments creating a temporary trench 50.8 ± 8 cm (20 ± 3 inch) deep; as the ripper tool moved across the basin, cable was fed into the temporary opening. This approach was critical to install the cable in dry sandy sediments where a stable trench cannot be created (for more details see Pham et al. 2017; O'Connell 2019). A second surface cable was placed on top of the backfilled trench and covered with a thin veneer of sediment to keep the cable in place and prevent damage from rodents. To maximize coverage, the cable was installed in a spiral pattern following the shape of the basin (Figure 1c). In the center of the basin, one end of the subsurface cable was installed vertically using direct push to a depth of ~9.0 m (29.5 feet) below-ground surface. The fiber optic cable (AFL Global, South Carolina) had two 50/125 µm multimode glass fibers with a 500 µm tight buffer, wrapped

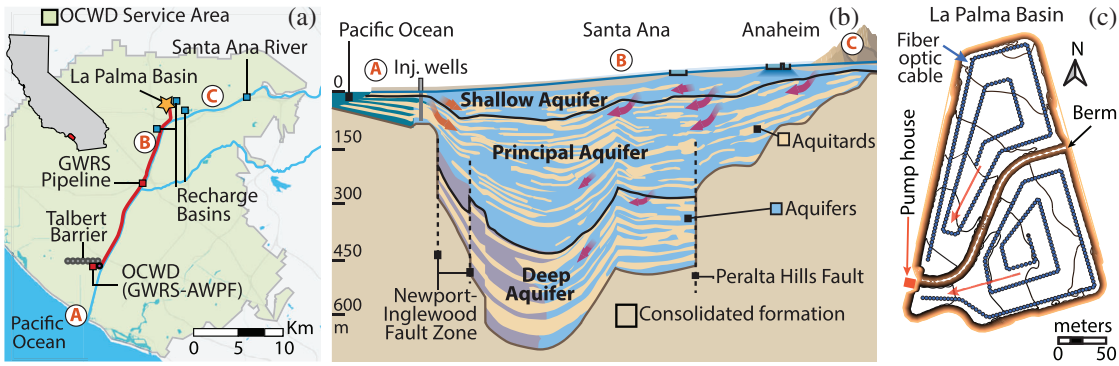

Figure 1. (a) Map showing OCWD service area. Approximately 20% to 30% of the advanced purified water produced by the GWRS-AWPF is injected into the Orange County Groundwater Basin at the Talbert Seawater Intrusion Barrier; the remaining water is sent inland to two spreading basins, Miraloma and La Palma Basins. (b) Geologic cross section showing the layers of the OC aquifer. The cross-section is along the Santa Ana River; the circled points A, B, and C are shown on the map (Figure 1a). (c) Schematic map of La Palma Basin (study site). The basin floor slopes from the northeast toward the southwest, indicated by the orange arrows. Blue circles delineate the location of co-located surface and subsurface fiber optic cables.

in a neoprene jacket. All four cables were connected to a single DTS unit (Silixa XT-DTS, Hertfordshire, United Kingdom). The DTS unit sends a coherent light (laser) signal through an individual fiber optic cable. As the light signal interacts with the fiberglass, light is scattered at different wavelengths that are below (anti-Stokes) and above (Stokes) the wavelength of the incident light signal. The ratio of anti-Stokes to Stokes is proportional to the temperature, while the time of flight gives the location along the cable (Selker et al. 2006; Becker et al. 2013). The DTS unit, averages the temperature along the cable every 25 cm (10 inch) for 10-min to improve accuracy. Measurements are collected every 15 min. The DTS unit and two calibration baths were housed inside a pump house, located adjacent to the basin, which provided power and security. Calibration baths are used to estimate parameters in the DTS temperature equation, which are then used to convert the measured anti-Stokes to Stokes ratio to temperature. Figure 2 shows an example of temperature recorded at the North sub-basin in November 2017. Panels *a* and *b* show the distributed temperature along the surface and subsurface cables, respectively. The diurnal temperature variation is evident in the vertical pattern observed, for example, yellow strips separated by blue strips. This diurnal pattern is observed in detail by plotting the average temperature across the entire cable; Figure 2c shows the average temperature for the week of November 5.

Measurement of Infiltration Rates at La Palma Basin

The average infiltration rate for the entire basin is estimated using the WB method, which treats the basin as a control volume, assumed to be at steady state over the integrating period. This method requires measuring the flow rate of water going into the basin and rate of change in storage to estimate the infiltration rate (e.g., flow rate out). Flow rate into La Palma Basin is measured using a 122 cm (48 inch) diameter electromagnetic flowmeter (Optiflux 4000, Krohne) and stage (surface water elevation) is measured using a transducer (HydroRanger 200, Siemens). A site-specific rating curve (stage vs. wetted area) is used to calculate the change in storage. Rainfall runoff does not significantly contribute to the flow going into the basin; therefore, runoff is ignored in the WB calculation. The maximum evaporation rate in Anaheim, California is approximately 8 mm/d (0.3 inch/d) in July to August (Hobbins et al. 2017). Using this rate, we estimate the maximum expected evaporated volume to be 0.03% of the average volume delivered to the basin, therefore, evaporation losses are ignored in this analysis. The WB provides a good estimate of the volume of water infiltrated by the basin, which can be converted to an average areal infiltration rate or water flux (feet/d). We calculated the maximum expected relative error (uncertainty) of the WB infiltration rate by assuming a combination of extreme but realistic values for the average flow rate, wetted area, and stage. The maximum relative uncertainty of WB infiltration rate is 5.0%, graphically represented by the light-blue shading in Figure 3b.

The use of heat as a tracer to estimate groundwater velocities is well documented in the literature. Vertical heat transport through a saturated porous media is described by the advection-dispersion equation for heat transport. The rate at which heat propagates vertically is proportional to the velocity of the infiltrating water by a retardation factor, $R \approx 2$ (Becker et al. 2013). This retardation factor is due to heat exchange with the sediment grains. Here we use diurnal temperature variations as a heat tracer to estimate infiltration rates. The phase shift in the diurnal signal between the two co-located temperature measurements can be related to the fluid velocity. We used a modified version of the cross wavelet transform algorithm (Grinsted et al. 2004; O'Connell 2019) to process the signals. An advantage of the cross wavelet transform over VFLUX (Gordon et al. 2012; Irvine et al. 2016), another popular method to process signals, is the ability to calculate phase shifts for time series containing mixed periodic signals. Using the cross wavelet transform, the phase shift is found

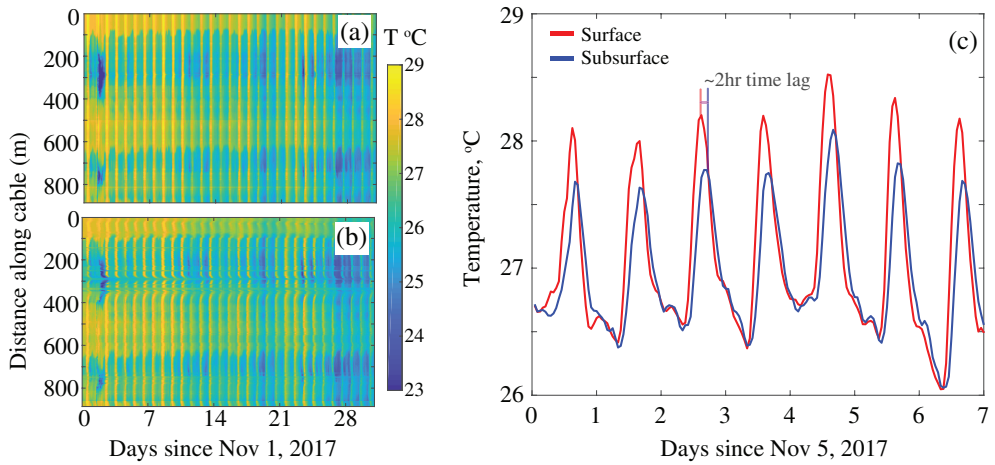

Figure 2. Recorded temperature along (a) surface and (b) sub-surface cable in the North sub-basin, November 2017, clearly showing a diurnal fluctuation. (c) Average temperature for the week of November 5 shows the temperature at the subsurface are dampened. The plot shows the subsurface signal has a time lag of ~2 h compared to the surface cable. The time-lag of the temperature peaks between the surface and subsurface cable is used to calculate the infiltration rate.

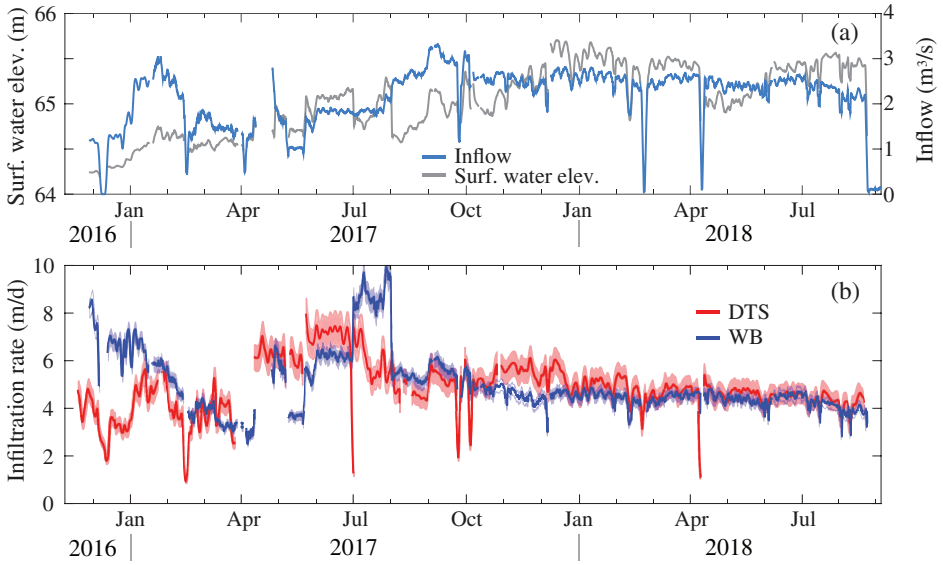

Figure 3. Historical performance data of La Palma basin. (a) Stage elevation (gray) and flow rate into La Palma Basin (light blue) and (b) infiltration rate measured using the WB method (blue) and basin averaged DTS (red). Note, the shaded region around the average WB infiltration rate represents the maximum uncertainty.

by convolving each temperature signal with the Morlet wavelet, at different scales, to localize the amplitude and phase of the diurnal signal, similar to the method used by Henderson et al. (2009). Once the diurnal signal is localized, the phase shift between the surface and subsurface signals is calculated. The phase shift is then used to calculate the time lag (t_{lag}), or the time it takes for a temperature signal to move distance d, from the surface to the subsurface cable. Using the lag time and accounting for the retardation factor, we calculate the velocity of the water. The velocity of water is then multiplied by the porosity (n_e) to calculate the infiltration rate, (q) as:

$$q = n_e v = n_e \frac{R * d}{t_{lag}} \quad (1)$$

This infiltration rate was calculated at each location along the cable. The relative uncertainty of the DTS infiltration rates was estimated to be about 8.9%, graphically represented by red shading in Figure 3b.

Results

We used 2 years of WB and temperature data, from November 2016 through August 2018, to estimate infiltration rates at the basin. La Palma Basin received advanced treated recycled water continuously since it was commissioned except for a few occasions when inflow was temporarily off for 12 to 96 h. Installing fiber optic cables before the basin was commissioned was advantageous to capture the infiltration dynamics from

the onset of basin operations and to establish baseline infiltration rates for a basin receiving treated water.

Basin-Averaged Infiltration Rates

During the initial months of La Palma Basin's operation, staff varied the inflow rate to assess the basin's response. Initially, the flow rate into the basin was 1.3 m^3/s (45 cfs) for approximately 1 month, the flow rate increased to 2.3 to 2.6 m^3/s (80 to 90 cfs) for the next 2 months and decreased to 1.4 m^3/s (50 cfs) the following 2 months. Figure 3a shows the inflow rate and the response of basin stage. The data exhibits daily, weekly, and seasonal fluctuations, which reflect variability in OCWD operations, for example, total output from the AWPF and volume of water injected at the sea water barrier, injection rates at wells, or flow rate delivered to other basins. Figure 3b shows the average infiltration rates measured using the WB (blue) and DTS (red) methods. Note the average rate from DTS is calculated by taking the arithmetic mean of locations submerged under water. Initially, average infiltration from the WB was estimated to be approximately 8.2 m/d (27 feet/d). From December 2016 to January 2017 the WB infiltration rate remained steady at 6.7 m/d (22 feet/d) and decreased rapidly to 2.7 m/d (9 feet/d) by April 2017. Surprisingly, the WB infiltration rates are not correlated with changes in the flow rate. For example, the infiltration rate decreased from January to April 2017, even when the flow rate was doubled from 1.3 to 2.6 m^3/s (45 to 90 cfs). In contrast, the DTS infiltration rates follow the same pattern as the flow rate into the basin, however, the DTS infiltration rates were lower (4.6 m/d or 15 feet/d) than WB in the initial stages of operations.

A second set of basin operation tests were conducted from April through July 2017 by alternating recharge between the North and South sub-basins. From April 4th through June 30th, the North sub-basin was off, and all water was diverted to the South sub-basin. During this period, the infiltration rate increased from 3.0 to 5.5 m/d (10 to 18 feet/d) as measured by WB and from 3.0 to 6.7 m/d (10 to 22 feet/d) as measured by DTS. During July 2017, flow was turned off to the South sub-basin and redirected to the North sub-basin. The North sub-basin WB infiltration rate increased to 8.5 m/d (28 feet/d), while the DTS infiltration rate decreased to 5.5 m/d (18 feet/d). We believe that the discrepancy between the DTS and WB infiltration rates is due to lateral flow. The times with the highest discrepancies (November to December 2016, April to May 2017, and July 2017), are also times when the flow rate of water going into the basin was rapidly adjusted or diverted to only one of the sub-basins. By keeping half of the basin empty and dry, flow can preferentially move both vertically and laterally (potentially traveling over clay lenses). The WB captures the increase in lateral flow, as evidenced by an increase in total infiltration, because the basin itself is the control volume, thus any lateral flow, either through the side-walls or in the subsurface, would be accounted for. The DTS method assumes one-dimensional vertical flow, and therefore, does not capture changes in lateral flow. It may also be possible that, when both sub-basins are operated concurrently, sub-surface lateral flow moving over clay lenses may create localized mounding or perching of the water table, however, more work is needed to confirm this.

After the alternating sub-basin experiment, both sub-basins were operated concurrently, from August 2017 to August 2018. During this period, the flow rate into the basin was 2.3 to 2.7 m^3/s (80 to 95 cfs). During this 12-month period, the magnitude of infiltration rates measured by both DTS and WB were within 10% of each other. The infiltration rate slowly decreased from 5.5 m/d (18 feet/d) to 4.0 m/d (13 feet/d). This decrease in infiltration rate is indicative of the basin bottom being clogged, which restricts flow and reduces the recharge rate.

Spatial Distribution of Infiltration Rates

Both WB and DTS methods provide useful information about the *overall* performance of the basin (e.g., basin-averaged infiltration rate) and the basin's response to changes in flow rate. However, the methods differ greatly in terms of spatial information and changes over time. As previously described, the WB method lumps the total infiltration into a single value, which represents the average infiltration rate and does not provide spatial information. In contrast, DTS measures the temperature at discrete points along the fiber optic cable, which are converted to infiltration rates. Thus, DTS provides significantly higher spatial resolution infiltration rates, limited only by the placement of the cable location. In this section, we discuss the results of spatially resolved infiltration rates obtained using DTS.

Figure 4 shows the spatial evolution of infiltration rates over 22 months after the basin was commissioned. The first two frames in Figure 4 show the basin floor was not fully submerged with water even though flow rate into the basin ranged from 1.3 to 2.6 m^3/s (45 to 90 cfs). In part, this was due to the extremely high infiltration rates recorded during the initial months of operation. In the first month of operation, only half of the basin floor was covered. During this month, the midsection of the South sub-basin had the highest infiltration rate. After 3 months, the basin floor was 80% submerged and some clear differences in spatial infiltration rates are observed between the first and third month of operation, suggesting fast-evolving infiltration dynamics. Interestingly, when flow was diverted to the South sub-basin only, the infiltration rate increased throughout the entire sub-basin. A similar effect was observed when flow was diverted to the North sub-basin only. We speculate that the reason for this observed increased infiltration rates throughout both sub-basins operating independently could be the increased head, for example, increased ponding depth. Another explanation for the increased infiltration rate when operating one sub-basin at a time is lateral flow from the filled sub-basin to the dry sub-basin, though more research is needed to confirm this.

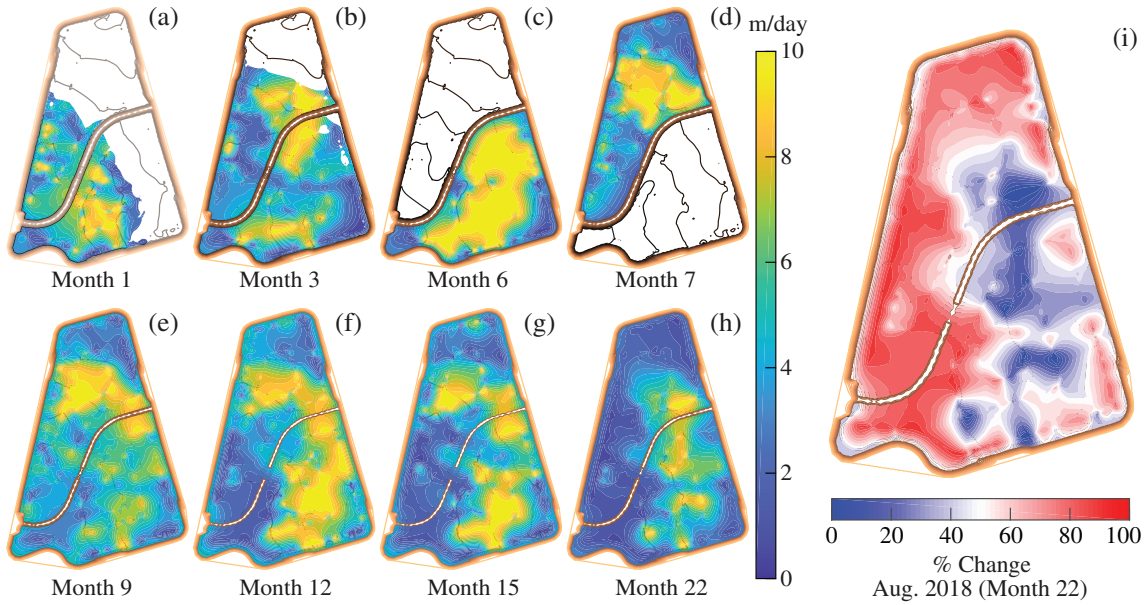

Figure 4. (a)–(h) Temporal evolution of spatially distributed infiltration rates at La Palma basin calculated using DTS. The basin remained partially filled for the first 3 months of operation. In month six and seven water was diverted to one sub-basin only, causing infiltration rates to increase slightly on the operational sub-basin. After the seventh month, both basins remained operational. The bottom row shows the progressive infiltration decline on the north and south-west corners of the basin. (i) Spatially distributed % change, relative to the maximum recorded DTS infiltration rate at each location, for August 2018. The % change map gives a better indication of how much the infiltration rate has declined throughout the basin.

The bottom row of Figure 4 shows the evolution over time with both sub-basins operating continuously for 12 months. These sub-figures show the spatial extent of high-infiltration regions slowly decreasing over time. DTS results show a high degree of spatial and temporal infiltration rate heterogeneity, which leads to the identification of high-performing and low-performing regions. For example, we observed that the middle of the North sub-basin and the eastern half of the South sub-basin are high-performing areas with infiltration rates ~7.6 to 10.6 m/d (25 to 35 feet/d). In contrast, the southwest and northeast are low-performing regions (~1.8 to 3.7 m/d or 6 to 12 feet/d). Additionally, it is clear the infiltration rate in the low-performing regions declined progressively, as indicated by those regions turning light blue to dark blue over time, for example, indicating near-zero infiltration rates. These results suggest that DTS spatial and temporal data can be used to identify regions where clogging is taking place. Typically, OCWD considers a basin clogged when the average infiltration rate has declined by 80% of its initial average infiltration rate. This suggests that after 22 months of operation, approximately 60% of the basin appears to have clogged (Figure 4i). The basin clogging can be visualized by calculating the infiltration rate percent change (%Δ) relative to the maximum recorded value at each location, calculated as $\%\Delta = (q_{max} - q_t)/q_{max}$, where q_{max} and q_t are the maximum and instantaneous DTS infiltration rates, respectively (Figure 4i). This figure highlights the spatial extent and severity of clogging throughout the basin. After 22 months of operation, the entire west side of the basin has decreased by approximately 80%, while the central-east side of the basin has only decreased between 20% and 40% of its maximum rate.

Cumulative Volume of Water Recharged by the Basin

Another way to quantify the overall performance of a basin is to calculate the cumulative volume of water recharged by the basin over time. Cumulative infiltrated volumes are typically reported by water agencies to inform the public. Comparing the volume recharged to the volume of water pumped out of the aquifer, is used to evaluate the level of stress or overdraft on the aquifer (Thomas et al. 2017). From a data processing perspective, cumulative volume of water recharged over the lifetime of the basin removes short-term flow rate and infiltration rate fluctuations and gives an overview of the basin's historical performance.

The volume of water infiltrated by the basin over the 22-month operating period was calculated using the WB and DTS methods. DTS total infiltrated volume was calculated by multiplying the localized infiltration rate (interpolated from a point every 4.0-m along the cable) times the surface area associated with that location (0.5 m by 0.5 m), and then integrating over time. WB infiltrated volume was calculated by multiplying the basin average infiltration rate by the total wetted area and integrating over time. For both methods, we accounted for wetted area by setting the infiltration rate of nonwetted areas equal to zero (see, e.g., Figure 4).

Figure 5 shows the cumulative volume of water infiltrated by La Palma Basin since it began operating in November 2016. Plotting cumulative volume is useful

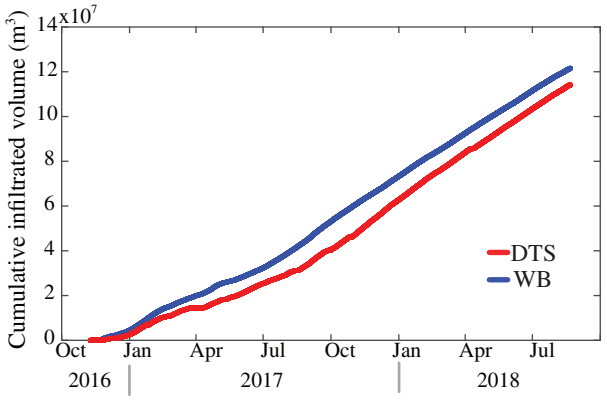

Figure 5. Cumulative infiltrated volume measured using WB (blue) and DTS (red). DTS infiltrated volume was estimated by interpolating infiltration rates throughout the basin. After August 2017, both methods estimate a similar rate of change of the total infiltrated volume.

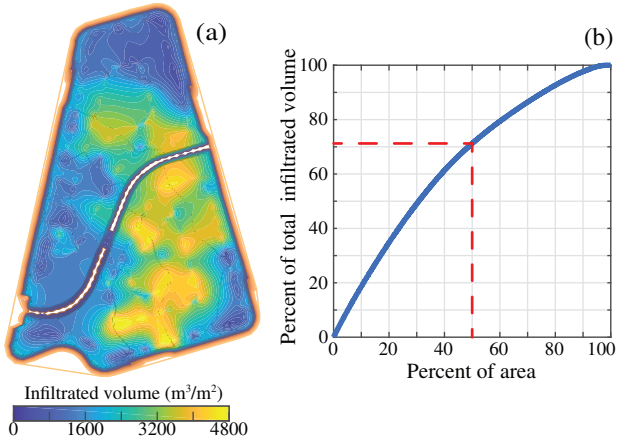

Figure 6. (a) Spatial distribution of cumulative infiltrated volume throughout the basin. (b) Cumulative infiltrated volume vs. the percent area of the basin, calculated from (a). The plot shows that 72% of the total volume of water infiltrated by the basin percolated through 50% of the basin area.

to evaluate the overall accuracy of DTS, since the WB method by default captures the cumulative recharge measured by inflow metering. Overall, the agreement verifies the general accuracy of DTS, despite periods of disagreement indicated earlier in Figure 3. Figure 5 shows that both methods capture the changes in cumulative recharged volume during the initial filling period and during the alternating sub-basin experiment; these changes are evidenced by the observed change in slope. The difference between the two methods is most notable in the early stages of the basin operations, as discussed previously for Figure 3. After August 2017, both DTS and WB cumulative recharge volume lines have the same slope, reinforcing the accuracy of DTS. By the end of August 2018, the total volume of water recharged was within a 5% relative difference, 121.6×10^6 m^3 (98,578 acre-feet) and 115.1×10^6 m^3 (93,300 acre-feet), for WB and DTS, respectively. The agreement between methods is highlighted by plotting the cumulative volume from August 2017 to 2018, after the basin toggling tests were completed (inset in Figure 5). Despite the significantly different underlying methods (i.e., inflow metering for WB vs. a fiber optic-based heat tracer algorithm for DTS), DTS appears to accurately measure cumulative volume of water recharged by the basin, and thus provides comparable information to conventional inflow metering methods while also allowing assessment of the spatial distribution of infiltration.

Because DTS provides location-specific infiltration rate, we can calculate the volume of water infiltrated in different parts of the basin. Figure 6a shows the spatially distributed cumulative infiltrated volume per square meter, throughout the basin. As expected, the distribution of cumulative infiltrated volume has a pattern similar to that observed in Figure 4, however, plotting the cumulative volume removes temporal variability and reveals long-term trends. The northeast corner infiltrated the least water, averaging about 600 m^3. The southwest region, on average, infiltrated about 1600 m^3. The central-eastern part of the basin infiltrated the highest volume of water, ranging from 3200 to 4800 m^3. Plotting the percent area vs. the fraction of water infiltrated revealed that 72% of the water percolated through 50% of the basin area (Figure 6b). Overall, this finding prompts a need to understand why certain regions of the basin provided high value while other regions were underperforming; furthermore, it provides a sense for the relative performance between areas over time.

Discussion

Continuously recording DTS data, for example, spatially distributed infiltration rates, from the start of basin operations helped monitor the basin performance through the initial 2 years of operation. The performance record was used to determine the maximum infiltration rates, study the evolution of performance over time, evaluate the effectiveness of different cleaning strategies, evaluate the total recharged volume of water, and quantify changes after consecutive basin cleaning, for example, after several cleaning cycles.

Using DTS Technology: Better Basin Management and Improved Cleaning Strategies

The spatial and temporal resolution of data obtained from DTS may benefit water agencies by providing near-real time infiltration rates. The accuracy of, and fast access to, data can be used to determine basin cleaning schedule. DTS data can also be used to determine whether to operate a single sub-basin or both sub-basins concurrently, and how much water to deliver to the basin and the ponding depth (stage) required to maximize infiltration rates.

The near-real-time capability and high-spatial resolution of DTS data may be used as a supplement to a supervisory control and data acquisition (SCADA) system. Such configuration can help plant operators know when

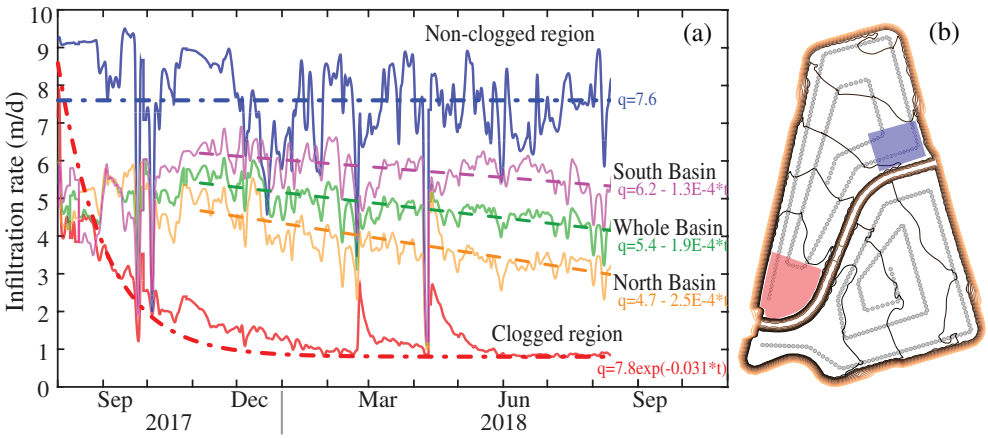

Figure 7. (a) Average infiltration rates for the whole basin (green), North sub-basin (orange), South sub-basin (magenta), clogged region (red), and nonclogged region (blue). Solid (fluctuating) lines are measured infiltration rates using DTS data and the dashed lines show the trendline. Approximate estimates were found by fitting the linear equation: $q(t) = q_0 - kt$ using a least squares method for all, except for the clogged region. The clogged region was estimated using an exponential function, $q(t) = q_0 e^{-mt}$, where $q(t)$ and q_0 are the infiltration rates (m/d) and k (m/d/d) and m (1/d) are the linear and exponential decay factors, respectively. (b) Basin map indicating the location of the clogged (red shade) and nonclogged (blue shade) regions.

the average infiltration rate of the basin has decreased enough to consider the basin clogged. As previously discussed, when a basin is clogged, remedial actions must be taken to restore or increase the infiltration rate of the basin. A common method used by OCWD is to physically remove the clogging sediment by scraping the bottom of the basin using heavy equipment, which produces several tons of unusable sediment. Depending on the size of the basin, the basin cleaning process can take up to 2 months, resulting in a loss of storage capacity and loss of recharge for that time. Furthermore, this process inadvertently removes clean native material along with the clogging sediment, making this practice unsustainable, for example, eventually clean sediment will be required to restore basin conditions.

Using the current instrumentation at La Palma basin, it is only possible to calculate the average infiltration rate for the two sub-basins combined (using the WB method). In contrast, the high-resolution DTS data can be used to monitor the average infiltration rate of the whole basin, single sub-basin, or even specific parts of the basin. For example, Figure 7 shows the averaged infiltration rates for the North sub-basin (orange), South sub-basin (magenta), and whole basin (green), from August 2017 to 2018. These infiltration rates appear to be linearly decreasing over the last 9 months. In addition to that, DTS can identify localized areas where the basin has clogged. For example, Figure 7b shows a clogged region (red) and nonclogged region (blue); the infiltration rate for these regions is shown in Figure 7a in red and blue, for the clogged and nonclogged region respectively. It is evident from the DTS data that the infiltration rate from either of these two regions has a significantly different behavior than the infiltration rates from the sub-basins or whole basin. Furthermore, the exponential infiltration rate decay in the southwest region (red region) indicated that the main mechanism responsible for the infiltration rate decay in this region is surface clogging, for example, formation of a clogging layer. This is further confirmed by the temporary spike and exponential decay during temporary flow shut-down. The level of detail and accuracy of DTS data can be used to evaluate whether a region within a basin has clogged and evaluate how severely it has clogged.

Spatially resolved infiltration rates from DTS, coupled with hydrogeologic information, may be used to differentiate between mounding and clogging (O'Connell 2019). Identifying the mechanism responsible for the rate decline, whether clogging or mounding, is important to utility managers because the remedial action depends on the cause. Furthermore, DTS-derived data opens the possibility for new basin-cleaning strategies, for example, *targeted cleaning*. The goal of targeted cleaning is to reduce basin operation downtime for cleaning while maximizing infiltration rates, by cleaning only those regions determined to be clogged. DTS data can be used to measure the infiltration rates over space and time, determine when the infiltration rate has decreased significantly, and decide on the proper remedial action. This level of data-driven management can reduce operation and maintenance costs, but more importantly, can increase the volume of water recharged by keeping the basin operating at its optimal condition.

Conclusion

Our experimental results show that DTS infiltration rate, averaged over the entire basin, were within a 5% relative difference to the control volume or WB method. Furthermore, the DTS infiltration rate matched the WB infiltration rate over an extended period (12 months). Differences in infiltration rates observed during the initial

months are not yet fully understood. Such differences could be caused by infiltration dynamics, lateral vadose flow, or side-wall infiltration; however, more research is needed to determine the cause for such behavior. Despite these differences during the initial months of recharge, the results obtained from the DTS provide a good measure of the average infiltration rate of the basin over the 2-year duration of this investigation. It was shown that high temporal and spatial resolution of measurements can be used to evaluate basin's performance in response to operator decisions. DTS infiltration monitoring can support data-driven decisions about basin cleaning schedule, frequency, and extent. Significantly, DTS information can also be used to assess historically high-performing and low-performing reaches of the basin allowing for targeted, and therefore more efficient, basin cleaning strategies. DTS technology was shown to provide comparable or better data than conventional methods for a lower equipment cost: the capital cost of DTS technology (about $40k for the unit and ~1.4$/m for the cable) is significantly lower than installing a flowmeter and SCADA-like instrumentation and requires less infrastructure. Incorporating DTS technology may lead to better basin management, reduced O&M costs, and increased volume of groundwater recharged into an aquifer.

Acknowledgments

This work was funded by the Orange County Water District. The authors would like to thank F. Day-Lewis and two anonymous reviewers for their insightful comments, which greatly improved this manuscript. The data used for this manuscript will be made available upon request.

Authors' Note

The authors do not have any conflicts of interest or financial disclosures to report.

References

Abel, C.D., R.C. Vortisch, J.P. Ntelya, S.K. Sharma, and M.D. Kennedy. 2015. Effect of primary effluent coagulation on performance of laboratory-scale managed aquifer recharge system. *Desalination and Water Treatment* 55, no. 6: 1413–1421.

Becker, M.W., B. Bauer, and A. Hutchinson. 2013. Measuring artificial recharge with fiber optic distributed temperature sensing. *Groundwater* 51, no. 5: 670–678.

Becker, M., T. Georgian, H. Ambrose, J. Siniscalchi, and K. Fredrick. 2004. Estimating flow and flux of ground water discharge using water temperature and velocity. *Journal of Hydrology* 296, no. 1: 221–233.

Bouwer, H. 2002. Artificial recharge of groundwater: Hydrogeology and engineering. *Hydrogeology Journal* 10, no. 1: 121–142.

Bouwer, H., and R.C. Rice. 1989. Effect of water depth in groundwater recharge basins on infiltration. *Journal of Irrigation and Drainage Engineering* 115, no. 4: 556–567.

Bouwer, H. 1988. Design and management of infiltration basins for artificial recharge of ground water. In *Proceedings of the 32nd Annual New Mexico Conference on Ground Water Management. Albuquerque, NM November 5–6, 1987*, 111–123. Las Cruces, New Mexico: New Mexico Water Resources Research Institute.

Bradshaw, J.L., M. Osorio, T.G. Schmitt, and R.G. Luthy. 2019. System modeling, optimization, and analysis of recycled water and dynamic storm water deliveries to spreading basins for urban groundwater recharge. *Water Resources Research* 55, no. 3: 2446–2463.

Briggs, M.A., L.K. Lautz, and J.M. McKenzie. 2012. A comparison of fibre-optic distributed temperature sensing to traditional methods of evaluating groundwater inflow to streams. *Hydrological Processes* 26, no. 9: 1277–1290.

Conant, B. 2004. Delineating and quantifying ground water discharge zones using streambed temperatures. *Groundwater* 42, no. 2: 243–257.

Constantz, J. 2008. Heat as a tracer to determine streambed water exchanges. *Water Resources Research* 44, no. 4., W0010.

Dillon, P., S. Toze, D. Page, J. Vanderzalm, E. Bekele, J. Sidhu, and S. Rinck-Pfeiffer. 2010. Managed aquifer recharge: Rediscovering nature as a leading-edge technology. *Water Science and Technology* 62, no. 10: 2338–2345.

Dillon, P. 2009. Water recycling via managed aquifer recharge in Australia. *Boletin Geologico y Minero* 120, no. 2: 121–130.

Dillon, P. 2005. Future management of aquifer recharge. *Journal of Hydrogeology* 13, no. 1: 313–316.

Drewes, J.E. 2009. Ground water replenishment with recycled water: Water quality improvements during managed aquifer recharge. *Groundwater* 47, no. 4: 502–505.

Fox, P., and R. Makam. 2011. Kinetics of model high molecular weight organic compounds biodegradation in soil aquifer treatment. *Water Research* 45, no. 15: 4419–4427.

Fox, P. (Ed). 2007. Management of aquifer recharge for sustainability. In *Proceedings of the 6th International Symposium on Managed Artificial Recharge of Groundwater, ISMAR6*. Phoenix, Arizona: Acacia Publishing Incorporated.

Gordon, R.P., L.K. Lautz, M.A. Briggs, and J.M. McKenzie. 2012. Automated calculation of vertical pore-water flux from field temperature time series using the VFLUX method and computer program. *Journal of Hydrology* 420: 142–158.

Grinsted, A., J.C. Moore, and S. Jevrejeva. 2004. Application of the cross wavelet transform and wavelet coherence to geophysical time series. *Non-linear Processes in Geophysics* 11: 561–566.

Hare, D.K., M.A. Briggs, D.O. Rosenberry, D.F. Boutt, and J.W. Lane. 2015. A comparison of thermal infrared to fiber-optic distributed temperature sensing for evaluation of groundwater discharge to surface water. *Journal of Hydrology* 530: 153–166.

Hatch, C.E., A.T. Fisher, J.S. Revenaugh, J. Constantz, and C. Ruehl. 2006. Quantifying surface water-groundwater interactions using time series analysis of streambed thermal records: Method development. *Water Resources Research* 42, no. 10. W10410.

Henderson, R.D., F.D. Day-Lewis, and C.F. Harvey. 2009. Investigation of aquifer estuary interaction using wavelet analysis of fiber-optic temperature data. *Geophysical Research Letters* 36: L06403.

Hobbins, M.T., J.J. Barsugli, C.F. Dewes, and I. Rangwala. 2017. Monthly pan evaporation data across the continental United States between 1950–2001. USGS Report, Reston, Virginia.

Hutchinson, A.S., G. Rodriguez, G. Woodside, and M. Milczarek. 2017. Maximizing infiltration rates by removing suspended solids: Results of demonstration testing of riverbed filtration in Orange County, California. *Water* 9, no. 2: 119.

Hutchinson, A., D. Phipps, G. Rodriguez, G. Woodside, and M. Milczarek. 2013. *Surface spreading recharge facility clogging—the orange county water district experience.*

Clogging Issues Associated with Managed Aquifer Recharge Methods, 107–118. Australia: IAH Commission on Managing Aquifer Recharge.

Irvine, D.J., M.A. Briggs, L.K. Lautz, R.P. Gordon, J.M. McKenzie, and I. Cartwright. 2016. Using diurnal temperature signals to infer vertical groundwater-surface water exchange. *Groundwater* 55, no. 1: 10–26.

Kazner, C., T. Wintgens, and P. Dillon. 2012. Water reclamation technologies for safe managed aquifer recharge. In *Water reclamation technologies for safe managed aquifer recharge*. IWA Publishing, London, UK.

Khadra, W.M., P.J. Stuyfzand, and I.M. Khadra. 2017. Mitigation of saltwater intrusion by integrated fresh-keeper wells combined with high recovery reverse osmosis. *Science of the Total Environment* 574: 796–805.

Koch, F.W., E.B. Voytek, F.D. Day-Lewis, R. Healy, M.A. Briggs, D. Werkema, and J.W. Lane Jr. 2015. 1DTempPro V2: New features for inferring groundwater/surface-water exchange. *Groundwater* 54: 434–439.

Lopez, O.M., K.Z. Jadoon, and T.M. Missimer. 2015. Method of relating grain size distribution to hydraulic conductivity in dune sands to assist in assessing managed aquifer recharge projects: Wadi Khulays Dune field, Western Saudi Arabia. *Water* 7, no. 11: 6411–6426.

Lowry, C.S., J.F. Walker, R.J. Hunt, and M.P. Anderson. 2007. Identifying spatial variability of groundwater discharge in a wetland stream using a distributed temperature sensor. *Water Resources Research* 43, no. 10. W10408.

Martin, R. 2013. Clogging issues associated with managed aquifer recharge methods. *IAH Commission on Managing Aquifer Recharge*.

Mawer, C., A. Parsekian, A. Pidlisecky, and R. Knight. 2016. Characterizing heterogeneity in infiltration rates during managed aquifer recharge. *Groundwater* 54, no. 6: 818–829.

Moore, N. 2014. *Geotechnical Evaluation La Palma Recharge Basin: Orange County Water District*. Ninyo & Moore Geotechnical and Environmental Sciences Consultants: Anaheim California.

Mwakanyamale, K., L. Slater, F. DayLewis, M. Elwaseif, and C. Johnson. 2012. Spatially variable stage-driven groundwater-surface water interaction inferred from time-frequency analysis of distributed temperature sensing data. *Geophysical Research Letters* 39, no. 6. L06401.

O'Connell, P.J. 2019. Differentiating clogging and mounding with distributed temperature sensing. Master's thesis, California State University, Long Beach, California.

Page, D., E. Bekele, J. Vanderzalm, and J. Sidhu. 2018. Managed aquifer recharge (MAR) in sustainable urban water management. *Water* 10, no. 3.

Pham, C., P.O.'. Connell, M. Becker, G. Rodriguez, A. Hutchinson, and M.H. Plumlee. 2017. Fiber optic distributed temperature sensing as a tool for measuring recharge rate in a potable reuse spreading basin. In *11TH IWA International conference on water reclamation and reuse*. The International Water Association, London.

Pidlisecky, A., and R. Knight. 2011. The use of wavelet analysis to derive infiltration rates from time-lapse one-dimensional resistivity records. *Vadose Zone Journal* 10, no. 2: 697–705.

Racz, A.J., A.T. Fisher, C.M. Schmidt, B.S. Lockwood, and M.L. Huertos. 2012. Spatial and temporal infiltration dynamics during managed aquifer recharge. *Groundwater* 50, no. 4: 562–570.

Rice, R.C. 1974. Soil clogging during infiltration of secondary effluent. *Journal of Water Pollution Control Federation* 46, no. 4: 708–716.

Selker, J.S., L. Thvenaz, H. Huwald, A. Mallet, W. Luxemburg, N.v.d. Giesen, M. Stejskal, J. Zeman, M. Westhoff, and M.B. Parlange. 2006. Distributed fiber-optic temperature sensing for hydrologic systems. *Water Resources Research* 42, no. 12. W12202.

Sherif, M.M., and K.I. Hamza. 2001. Mitigation of seawater intrusion by pumping brackish water. *Transport in Porous Media* 43, no. 1: 29–44.

Silliman, S.E., J. Ramirez, and R.L. McCabe. 1995. Quantifying downflow through creek sediments using temperature time series: One-dimensional solution incorporating measured surface temperature. *Journal of Hydrology* 167, no. 1: 99–119.

Stallman, R.W. 1965. Steady one-dimensional fluid flow in a semi-infinite porous medium with sinusoidal surface temperature. *Journal of Geophysical Research* 70, no. 12: 2821–2827.

Suzuki, S. 1960. Percolation measurements based on heat flow through soil with special reference to paddy fields. *Journal of Geophysical Research* 65, no. 9: 2883–2885.

Taniguchi, M. 1993. Evaluation of vertical groundwater fluxes and thermal properties of aquifers based on transient temperature-depth profiles. *Water Resources Research* 29, no. 7: 2021–2026.

Thomas, B.F., J.S. Famiglietti, F.W. Landerer, D.N. Wiese, N.P. Molotch, and D.F. Argus. 2017. Grace groundwater drought index: Evaluation of California central valley groundwater drought. *Remote Sensing of Environment* 198: 384–392.

Tyler, S.W., J.S. Selker, M.B. Hausner, C.E. Hatch, T. Torgersen, C.E. Thodal, and S.G. Schladow. 2009. Environmental temperature sensing using Raman spectra DTS fiber-optic methods. *Water Resources Research* 45, no. 4. W00D23.

Vogt, T., P. Schneider, L. Hahn-Woernle, and O.A. Cirpka. 2010. Estimation of seepage rates in a losing stream by means of fiber-optic high-resolution vertical temperature profiling. *Journal of Hydrology* 380, no. 1: 154–164.

Woodside, G., and M. Westropp 2015. Orange County water district groundwater management plan 2015 update. Technical report, Orange County Water District.